

AN ULTRASOFT X-RAY FLARE FROM 3XMM J152130.7+074916: A TIDAL DISRUPTION EVENT CANDIDATE

DACHENG LIN¹, PETER W. MAKSYM², JIMMY A. IRWIN², S. KOMOSSA³, NATALIE A. WEBB^{4,5}, OLIVIER GODET^{4,5}, DIDIER BARRET^{4,5}, DIRK GRUPE⁶, STEPHEN D. J. GWYN⁷

Draft version July 16, 2018

ABSTRACT

We report on the discovery of an ultrasoft X-ray transient source, 3XMM J152130.7+074916. It was serendipitously detected in an *XMM-Newton* observation on 2000 August 23, and its location is consistent with the center of the galaxy SDSS J152130.72+074916.5 ($z = 0.17901$ and $d_L = 866$ Mpc). The high-quality X-ray spectrum can be fitted with a thermal disk with an apparent inner disk temperature of 0.17 keV and a rest-frame 0.24–11.8 keV unabsorbed luminosity of $\sim 5 \times 10^{43}$ erg s⁻¹, subject to a fast-moving warm absorber. Short-term variability was also clearly observed, with the spectrum being softer at lower flux. The source was covered but not detected in a *Chandra* observation on 2000 April 3, a *Swift* observation on 2005 September 10, and a second *XMM-Newton* observation on 2014 January 19, implying a large variability (>260) of the X-ray flux. The optical spectrum of the candidate host galaxy, taken ~ 11 yrs after the *XMM-Newton* detection, shows no sign of nuclear activity. This, combined with its transient and ultrasoft properties, leads us to explain the source as tidal disruption of a star by the supermassive black hole in the galactic center. We attribute the fast-moving warm absorber detected in the first *XMM-Newton* observation to the super-Eddington outflow associated with the event and the short-term variability to a disk instability that caused fast change of the inner disk radius at a constant mass accretion rate.

Subject headings: accretion, accretion disks — galaxies: individual: 3XMM J152130.7+074916 — galaxies: nuclei — X-rays: galaxies.

1. INTRODUCTION

When stars wander too close to the supermassive black holes (SMBHs), which are believed to be present in the center of most massive galaxies, they could be disrupted and subsequently accreted, leading to energetic flares (Lidskii & Ozernoi 1979; Rees 1988, 1990). Such tidal disruption events (TDEs) provide a unique way to find and study otherwise dormant SMBHs in galactic nuclei. TDEs involving solar-type stars are expected to rise very fast (less than a few months) and decay for months to years, approximately as $t^{-5/3}$, after a period of peak accretion at a super-Eddington rate. The spectrum is expected to be ultrasoft, with characteristic temperatures of $\lesssim 0.1$ keV, thus mostly in UV to soft X-rays. The peak X-ray luminosity L_X can reach around 10^{44} erg s⁻¹. Most candidates discovered thus far belong to such soft TDEs (e.g., Grupe et al. 1999; Komossa & Greiner 1999; Komossa & Bade 1999; Esquej et al. 2008; Lin et al. 2011; Maksym et al. 2010, 2013, 2014a; Donato et al. 2014). A couple of hard TDEs with strong hard X-ray emission (peak isotropic

X-ray luminosity $>10^{47}$ erg s⁻¹) were also found recently and attributed to the presence of a relativistic jet in the events (Bloom et al. 2011; Burrows et al. 2011; Cenko et al. 2012). We refer to Komossa (2012) and Komossa (2015) for recent reviews of TDEs in X-rays.

There are other X-ray transients reaching X-ray luminosities comparable to those of TDEs around SMBHs. However, their duration and lightcurve evolution is typically very different. The X-ray afterglow of γ -ray bursts (GRBs) can have peak $L_X \sim 10^{51}$ erg s⁻¹ and last for months (e.g., Levan et al. 2014) or, in a few cases, for years (e.g., Grupe et al. 2010). Their X-ray spectra are generally hard with photon index $\lesssim 2$ (Grupe et al. 2013). Recently, several ultralong GRBs were discovered, with the late-time X-ray spectra found to be very soft (photon index >3 , e.g., Piro et al. 2014; Margutti et al. 2015). While supernovae (SNe) seldom have L_X above 10^{42} erg s⁻¹ (e.g., Immler 2007; Levan et al. 2013), the superluminous supernova SCP 06F6 was detected in X-rays ~ 150 days after its initial discovery, with $L_X \sim 10^{45}$ erg s⁻¹. Soderberg et al. (2008) also serendipitously discovered an extremely luminous X-ray outburst from SN 2008D, with peak $L_X \sim 6 \times 10^{43}$ erg s⁻¹. The main event, however, lasted only several hundred seconds and could arise from the prompt shock breakout from the SN progenitor's surface. The outburst showed a significant hard-to-soft spectral evolution, with photon index ~ 1.7 , typical of SNe, at the peak, to ~ 3.2 about 400 s later.

In our continuing effort to classify X-ray sources serendipitously detected by *XMM-Newton* and *Chandra* (e.g., Lin et al. 2012, 2014), we discovered a supersoft X-ray transient 3XMM J152130.7+074916 (J1521+0749 hereafter) in the *XMM-Newton* Serendipitous Source

¹Space Science Center, University of New Hampshire, Durham, NH 03824, USA, email: dacheng.lin@unh.edu

²Department of Physics and Astronomy, University of Alabama, Box 870324, Tuscaloosa, AL 35487, USA

³Max-Planck-Institut für Radioastronomie, Auf dem Hügel 69, 53121 Bonn, Germany

⁴CNRS, IRAP, 9 avenue du Colonel Roche, BP 44346, F-31028 Toulouse Cedex 4, France

⁵Université de Toulouse, UPS-OMP, IRAP, Toulouse, France

⁶Space Science Center, Morehead State University, 235 Martindale Drive, Morehead, KY 40351, USA

⁷Canadian Astronomy Data Centre, Herzberg Institute of Astrophysics, 5071 West Saanich Road, Victoria, British Columbia, V9E 2E7, Canada

Catalog (the 3XMM-DR5 version, Rosen et al. 2015). The source seems to show an X-ray outburst in 2000. In this paper, we report the properties of this source and argue that it is probably a soft TDE at a redshift of $z = 0.17901$ (the source luminosity distance $d_L = 866$ Mpc, assuming a flat universe with $H_0=70$ km s $^{-1}$ Mpc $^{-1}$ and $\Omega_M=0.3$). In Section 2, we describe the data analysis of *XMM-Newton*, *Chandra*, *Swift* and *ROSAT* observations. In Section 3, we first identify the host galaxy of our source, followed by the presentation of its detailed X-ray spectral and timing properties. We discuss the nature of our source and give conclusions of our study in Section 4.

2. DATA ANALYSIS

Table 1 lists all the pointed X-ray observations that covered J1521+0749 and were analyzed by us. There are two *XMM-Newton* observations, one *Chandra* observation, one *Swift* observation, and two *ROSAT* observations. They are denoted as X1, X2, C1, S1, R1 and R2, respectively, hereafter (refer to the table). All these observations have the cluster of galaxies MKW 3s as the target, with J1521+0749 observed at off-axis angles of $\sim 6''-9''$. J1521+0749 was serendipitously detected in X1 but not in the other observations. We extracted the spectrum and light curve from X1 for detailed study. We also extracted the spectra and the corresponding response files for the other observations in order to constrain the luminosity level of our source in these observations. Circular regions (see Table 1 for the radii used) were used to extract the source spectra. Our source is relatively far away from MKW 3s, but there is still some small contamination of the X-ray emission from this cluster of galaxies on our source. In order to accurately represent the contamination level, we extracted the background spectra from 4–8 circular regions that are near our source and had the same size and the same distance to MKW 3s as the source region. Below we give more details about the procedures that we adopted in analysis of each observation.

The source was in the field of view (FOV) of all the three European Photon Imaging Cameras (i.e., pn, MOS1, and MOS2, Jansen et al. 2001; Strüder et al. 2001; Turner et al. 2001) in the imaging mode in both *XMM-Newton* observations. We used SAS 13.5.0 and the calibration files of 2014 August for reprocessing the X-ray event files and follow-up analysis. The data in strong background flare intervals, seen in all cameras in X1 and in the pn camera in X2, were excluded following the SAS thread for the filtering against high backgrounds, i.e., excluding all times when the background level exceeded the low and steady level⁸. The final exposures used are given in Table 1. In the end we used 73%, 81%, and 81% of the total exposures of pn, MOS1, and MOS2 for X1, respectively. The corresponding fractions are 97%, 100%, and 100% for X2, respectively. The event selection criteria that we adopted followed the default values in the pipeline (see Table 5 in Watson et al. 2009). J1521+0749 was also covered in the Optical Monitor (OM, Mason et al. 2001) in both observations. In X1, the *UVW1* (2910 Å), *U* (3440 Å), *B* (4500 Å), and *V*

(5430 Å) filters were used, while in X2, two more filters, *UVW2* (2120 Å) and *UVM2* (2310 Å), were used. We used the SAS task *omichain* to obtain the photometry of our source (Table 2).

The C1 observation used the imaging array of the AXAF CCD Imaging Spectrometer (ACIS; Bautz et al. 1998). Our source is in the front-illuminated chip I2. We reprocessed the data to apply the latest calibration (CALDB 4.5.9) using the script *chandra_repro* in the *Chandra* Interactive Analysis of Observations (CIAO, version 4.6) package. We used a source extraction region enclosing 70% of the point spread function.

In the S1 observation, the X-ray telescope (XRT; Burrows et al. 2005) was operated in Photon Counting mode for 9.6 ks, and the UV-Optical Telescope (UVOT; Roming et al. 2005) used the *UVW1* filter (2910 Å) for 8.9 ks. We analyzed the data with FTOOLS 6.16 and the latest calibration files (XRT 20140730 and UVOT 20130118). The X-ray data were reprocessed with the task *xrtpipeline* (version 0.13.1) to update the calibration. Other than estimating the luminosity level of our source in the XRT, we also calculated the UV emission level with the task *uvotsource*, using radii of 5'' and 20'' for the circular source and background regions, respectively.

The *ROSAT* observations were also analyzed with FTOOLS 6.16. We note that there are three more *ROSAT* pointed observations that covered J1521+0749. We did not include them in this study because they are not deep enough to provide good constraints on the flux limits of our source, due to large off-axis angles and/or short exposures. J1521+0749 was not detected either in these observations.

3. RESULTS

3.1. The X-ray Source Position and the Host Galaxy

The position of J1521+0749 in the 3XMM-DR5 catalog is only 0'06'' away from the Sloan Digital Sky Survey (SDSS, Abazajian et al. 2009) galaxy SDSS J152130.72+074916.5 (Figure 1). However, such a small offset could be an artifact to some extent, considering that this source was among those used for the absolute astrometry correction and that it is one of the brightest sources in X1. Therefore, we recalculated the source position. We first obtained the mean positions (weighted by the uncertainties) of the point sources in X1, X2 and C1, after correcting the astrometry of X2 and C1 relative to X1 using the SAS task *catcorr*. For C1, we included a systematic uncertainty of 0'16'' obtained in Rots & Budavári (2011). The task *catcorr* also calculated the systematic positional uncertainties from the astrometric rectification procedure (Rosen et al. 2015). Such systematic uncertainties were taken into account and propagated. The mean positions, excluding J1521+0749 and those in bright X-ray emission from MKW 3s, were then cross-correlated with optical sources to obtain the absolute astrometry correction. For the optical sources, we stacked the Canada-France-Hawaii Telescope (CFHT) MegaPrime/MegaCam (Boulade et al. 2003) images (aligned to the SDSS astrometry) in the r' band taken between 2008 April and 2010 April using MegaPipe (Gwyn 2008), resulting in a total exposure of 3840 s

⁸ http://xmm.esac.esa.int/sas/current/documentation/threads/EPIC_filterbackground.shtml

TABLE 1
THE X-RAY OBSERVATION LOG

Obs. ID	Date	Detector	OAA	T	r_{src}	Count rate	L_{abs}	L_{unabs}
(1)	(2)	(3)	(4)	(ks)	(6)	(10^{-3} counts s^{-1})	(10^{43} erg s^{-1})	(10^{43} erg s^{-1})
(7)	(8)	(9)						
<i>XMM-Newton</i> :								
0109930101(X1)	2000-08-23	pn/MOS1/MOS2	9.2'	31/41/41	25''/25''/25''	$80.6 \pm 2.7/16.1 \pm 1.1/19.5 \pm 1.2$	$3.45^{+0.16}_{-0.29}$	$5.28^{+2.28}_{-1.00}$
0723801501(X2)	2014-01-19	pn/MOS1/MOS2	8.6'	96/117/117	10''/10''/10''	< 0.17/< 0.18/< 0.12	< 0.01	< 0.02
<i>Chandra</i> :								
900(C1)	2000-04-03	ACIS-I2	7.6'	57	5.1''	< 0.06	< 0.03	< 0.04
<i>Swift</i> :								
00035189001(S1)	2005-09-10	XRT	6.2'	9.6	20''	< 0.36	< 0.27	< 0.42
<i>ROSAT</i> :								
rp800128n00(R1)	1992-08-15	PSPCB	6.2'	9.6	30''	< 0.99	< 0.12	< 0.19
rh800425n00(R2)	1994-08-23	HRI	6.2'	13.4	10''	< 0.41	< 0.22	< 0.33

NOTE. — Columns: (1) the observation ID with our designation given in parentheses, (2) the observation start date, (3) the detector, (4) the off-axis angle, (5) the exposures of data used in final analysis, (6) the radius of the source extraction region, (7) the net count rate (0.2–2 keV for *XMM-Newton* observations, 0.3–2 keV for *Swift* and *Chandra* observations, and 0.1–2.4 keV for *ROSAT* observations, all in the observer frame), (8) rest-frame 0.24–11.8 keV luminosity, corrected for Galactic absorption but not intrinsic absorption, (9) rest-frame 0.24–11.8 keV luminosity, corrected for all neutral and ionized absorption. The spectral shape obtained for X1 using the MCD model subject to a fast-moving warm absorber was assumed in calculation of the luminosities for other observations. All uncertainties and upper bounds are at the 90% confidence level, calculated using the Bayesian approach with the CIAO task *aprates* for all observations except X1.

TABLE 2
THE *XMM-Newton*/OM PHOTOMETRY OF J1521+0749

Obs	UVW2	UVM2	UVW1	U	B	V
X1	> 20.0	> 20.4	21.5 ± 0.5	20.3 ± 0.5
X2	> 18.5	> 19.4	> 20.4	> 20.6	21.2 ± 0.4	20.2 ± 0.3

NOTE. — The AB magnitudes with 1σ uncertainties or the 3σ detection limits are given.

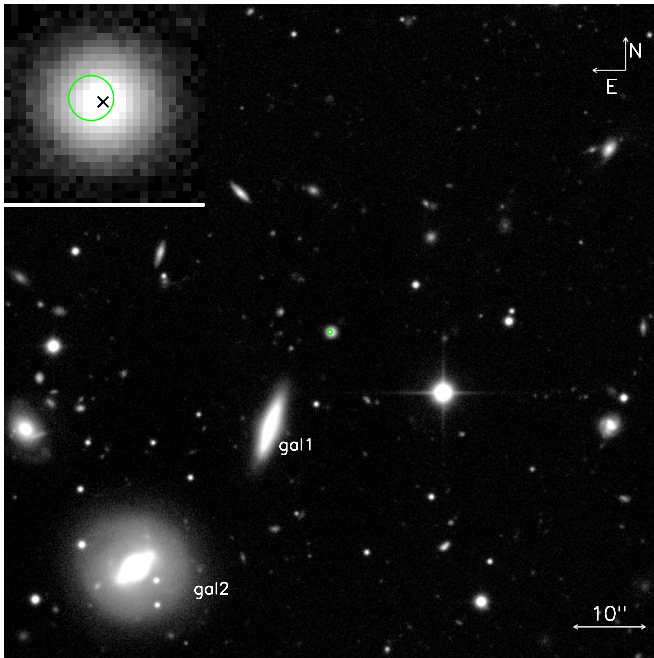


FIG. 1.— The CFHT/MegaPrime r' -band image around the field of J1521+0749. The green circle of radius $0''.58$ (i.e., 1.8 kpc) represents the 99% positional uncertainty of J1521+0749, indicating that J1521+0749 is consistent with the center of the galaxy SDSS J152130.72+074916.5. The two closest galaxies to J1521+0749 in MKW 3s are SDSS J152131.80+074851.9 and SDSS J152134.15+074815.3 ('gal1' and 'gal2' in the plot, respectively). The inset plot in the upper left corner zooms in on the $5'' \times 5''$ region around SDSS J152130.72+074916.5. The center of the galaxy is marked with a cross.

and a median seeing FWHM of $0''.77$. The new absolute astrometry correction gave the position of J1521+0749 to be R.A.=15:21:30.75 and Decl.=+7:49:16.7, with the 99% positional uncertainty of $0''.58$ (i.e., 1.8 kpc at the redshift $z = 0.17901$ of the candidate host galaxy of J1521+0749; see below). The relatively small positional uncertainty is mostly thanks to the very high quality of the X1 detection. This new position is $0''.33$ away from the center of SDSS J152130.72+074916.5, consistent within the uncertainty (Figure 1). The number density of the optical sources that are as bright as or brighter than SDSS J152130.72+074916.5 in the r' band within $10'$ is 0.00038 per square arcsec. Thus the chance probability for our X-ray source to be within $0''.33$ from the center of SDSS J152130.72+074916.5 is only 0.0001.

The SDSS took a spectrum of the galaxy on 2011 May 28, which is shown in Figure 2 (from the SDSS archive). Although the spectrum is a little noisy, the typical absorption features indicating a non-active galaxy can be seen. The redshift of the galaxy is $z = 0.17901 \pm 0.00007$ ($D_L = 866$ Mpc). No clear emission lines, except some spikes due to contamination from sky lines, can be seen. The 3σ upper limit of the flux of [O III] $\lambda 5007$ is 1.8×10^{-17} erg s^{-1} cm^{-2} , corresponding to a luminosity of 1.6×10^{39} erg s^{-1} (Galactic extinction corrected). Using the bolometric correction factors from the [O III] $\lambda 5007$ flux in Lamastra et al. (2009), we obtained the 3σ upper limit of the bolometric luminosity of the persistent nuclear activity to be 1.4×10^{41} erg s^{-1} .

In order to examine the host galaxy properties in greater detail, we fitted the SDSS spectrum to multi-component models comprised of single-population synthetic spectra, as in Maksym et al. (2014b). Using Penalized Pixel Fitting (PPXF) software (Cappellari & Emsellem 2004) and Vazdekis et al. (2010) synthetic spectra spanning a grid of 48 ages up to 14 Gyr, with $[M/H]=\{+0.22, 0.00, -0.40, -0.71, -1.31, -1.71\}$, we found that J1521+0749 is consistent with an old ($\gtrsim 10$ Gyr), passive stellar population. Full-spectrum kinematics implied a stellar dispersion $\sigma_* \sim 66$ km s^{-1} , which is comparable to the limit

TABLE 3
FITTING RESULTS OF THE X1 SPECTRUM FROM J1521+0749

Models	MCD+Ga ^a	BB+Ga ^b
$N_{H,i}$ (10^{20} cm ⁻²)	$0.3^{+1.4}$	$0.0^{+0.4}$
kT_{MCD}/kT_{BB} (keV)	$0.125^{+0.005}_{-0.006}$	$0.099^{+0.002}_{-0.003}$
N_{MCD}/N_{BB}	216^{+101}_{-46}	629^{+106}_{-76}
E_{ga} (keV)	$0.75^{+0.02}_{-0.07}$	$0.76^{+0.02}_{-0.03}$
σ_{ga} (keV)	$0.02^{+0.06}$	$0.00^{+0.05}$
N_{ga} (10^{-5})	$1.0^{+1.1}_{-0.20}$	$0.8^{+0.5}_{-0.3}$
L_{abs} (10^{43} erg s ⁻¹) ^b	$3.48^{+0.29}_{-0.20}$	$3.20^{+0.13}_{-0.13}$
L_{unabs} (10^{43} erg s ⁻¹) ^c	$3.65^{+0.58}_{-0.24}$	$3.20^{+0.17}_{-0.13}$
L_{bol} (10^{43} erg s ⁻¹) ^d	$7.40^{+1.64}_{-0.63}$	$4.24^{+0.26}_{-0.21}$
C/ν^e	536.4/528	545.9/528
Models	edge*MCD	edge*BB
$N_{H,i}$ (10^{20} cm ⁻²)	$0.0^{+0.6}$	$0.0^{+0.4}$
kT_{MCD}/kT_{BB} (keV)	$0.144^{+0.008}_{-0.006}$	$0.106^{+0.004}_{-0.003}$
N_{MCD}/N_{BB}	105^{+28}_{-20}	458^{+81}_{-74}
E_{edge} (keV)	$0.85^{+0.02}_{-0.02}$	$0.84^{+0.03}_{-0.03}$
τ_{edge}	$0.98^{+0.35}_{-0.32}$	$0.52^{+0.32}_{-0.30}$
L_{abs} (10^{43} erg s ⁻¹) ^b	$3.35^{+0.15}_{-0.15}$	$3.07^{+0.13}_{-0.13}$
L_{unabs} (10^{43} erg s ⁻¹) ^c	$3.46^{+0.21}_{-0.13}$	$3.13^{+0.13}_{-0.13}$
L_{bol} (10^{43} erg s ⁻¹) ^d	$6.32^{+0.55}_{-0.36}$	$4.04^{+0.21}_{-0.20}$
C/ν^e	529.7/529	552.8/529
Models	zxipcf*MCD	zxipcf*BB
$N_{H,i}$ (10^{20} cm ⁻²)	$0.0^{+1.6}$	$0.0^{+0.6}$
kT_{MCD}/kT_{BB} (keV)	$0.169^{+0.024}_{-0.017}$	$0.130^{+0.007}_{-0.007}$
N_{MCD}/N_{BB}	72^{+36}_{-20}	577^{+97}_{-78}
$N_{H,zxipcf}$ (10^{22} cm ⁻²)	$4.7^{+2.7}_{-1.2}$	$2.8^{+1.3}_{-0.6}$
$\log \xi_{zxipcf}$	$2.02^{+0.10}_{-0.09}$	$1.29^{+0.09}_{-0.09}$
z_{zxipcf}	$-0.12^{+0.02}_{-0.02}$	$-0.12^{+0.02}_{-0.03}$
L_{abs} (10^{43} erg s ⁻¹) ^b	$3.45^{+0.16}_{-0.29}$	$3.20^{+0.14}_{-0.14}$
L_{unabs} (10^{43} erg s ⁻¹) ^c	$5.28^{+2.28}_{-1.90}$	$9.94^{+3.67}_{-2.56}$
L_{bol} (10^{43} erg s ⁻¹) ^d	$8.6^{+3.2}_{-1.3}$	$11.6^{+4.1}_{-2.8}$
C/ν^e	523.8/528	532.1/528
Models	zxipcf*optxagnf _{Sch} ^f	zxipcf*optxagnf _{Kerr} ^g
$N_{H,i}$ (10^{20} cm ⁻²)	$0.0^{+1.6}$	$0.0^{+1.6}$
M_{BH} (M_{\odot})	$1.9^{+0.4}_{-0.4} \times 10^5$	$1.4^{+0.3}_{-0.3} \times 10^6$
L_{Bol}/L_{Edd}	$4.2^{+1.9}_{-1.0}$	$0.51^{+0.28}_{-0.12}$
$N_{H,zxipcf}$ (10^{22} cm ⁻²)	$4.7^{+2.7}_{-2.3}$	$4.7^{+2.7}_{-2.3}$
$\log \xi_{zxipcf}$	$2.02^{+0.15}_{-0.09}$	$2.02^{+0.13}_{-0.07}$
z_{zxipcf}	$-0.12^{+0.02}_{-0.02}$	$-0.12^{+0.02}_{-0.03}$
C/ν^e	523.7/528	523.7/528

NOTE. — All fits used the C statistic. ^a“Ga” is a Gaussian emission line; ^brest-frame 0.24–11.8 keV luminosity, corrected for Galactic absorption but not intrinsic absorption; ^crest-frame 0.24–11.8 keV luminosity, corrected for all neutral and ionized absorption; ^dthe bolometric luminosity based on the total flux of the thermal component (MCD or BB); ^ethe C statistic and the degrees of freedom; ^ffor thermal emission from an accretion disk around a non-rotating Schwarzschild BH; ^gfor thermal emission from an accretion disk around a maximally rotating Kerr BH.

from SDSS instrumental dispersion $\sigma_{*} \sim 69$ km s⁻¹. We likewise modeled the spectrum with STARLIGHT and two arrays of Bruzual & Charlot (2003) synthetic spectra, as in Maksym et al. (2014b). STARLIGHT inferred a stellar mass $M_{*} \sim 8.4 \times 10^9 M_{\odot}$. Care should be taken in interpreting σ_{*} , since in general S/N $\lesssim 10$ for $\lambda \lesssim 5400$ Å (rest-frame). Using Graham & Scott (2015), we inferred the central BH mass $M_{BH} \sim 2 \times 10^7 M_{\odot}$, which has a 1σ uncertainty of 0.83 dex. The BH mass can also be estimated using the BH mass versus bulge K -band luminosity relation (Graham 2007; Marconi & Hunt 2003) and is $\lesssim 5 \times 10^7 M_{\odot}$, based on the K -band magnitude of $m_K = 16.99$ ($M_K = -22.4$) of the galaxy from the the 3.8m United Kingdom Infra-red Telescope (UKIRT) Infrared Deep Sky Survey (Lawrence et al. 2007). These BH mass estimates are consistent with each other and are a little larger than the estimate from the X-ray spectral

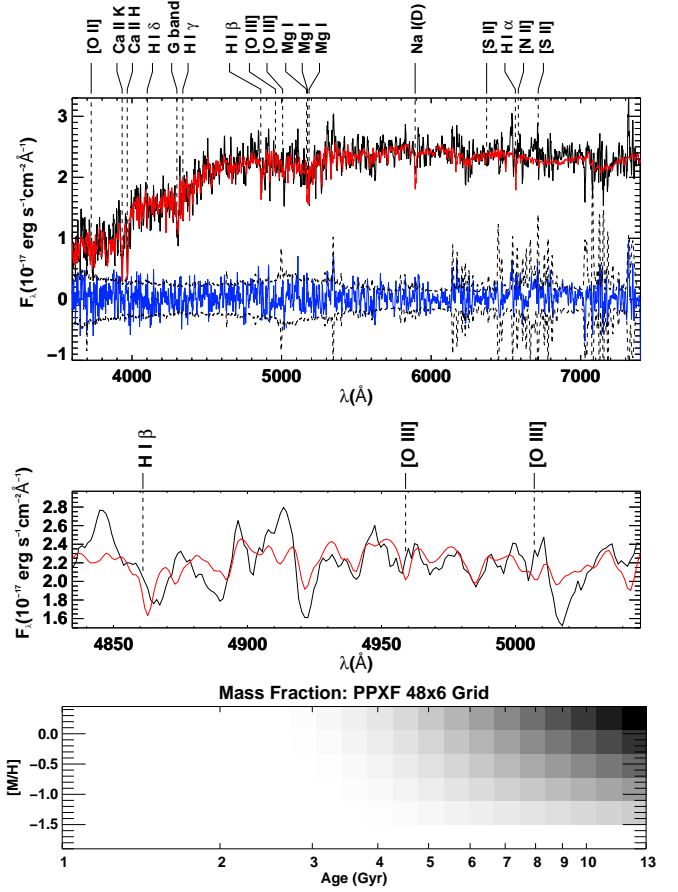


FIG. 2.— Top panel: PPF best-fit modeling of J1521+0749. The SDSS rest-frame data (black, solid) are overplot with the best-fit PPF model (red). Points are smoothed with a boxcar function over 5 pixels for clarity. Smoothed residuals are also plotted (blue) with mean noise (black, dashed). A strong O I $\lambda 5577$ Å (observed) sky line has been masked out. Important stellar absorption and AGN diagnostic emission lines are overplot for reference. Note that several strong false ‘features’ are associated with atmospheric OH complexes at long λ , particularly near H α $\lambda 6563$ Å. Middle panel: As with the top, with the region about [O III] expanded for clarity and emphasis. Bottom panel: Relative mass fractions of different stellar populations with respect to metallicity and age, as per the best-fit model the PPF template synthesis code. Dominant populations are indicated by shading, with darker shading indicating a larger fraction of the total stellar mass in the best-fit model.

fit in Section 3.3 ($\sim 10^5$ – $10^6 M_{\odot}$).

3.2. The Long-term Variability

Figure 3 plots the long-term evolution of the unabsorbed luminosity L_X of J1521+0749 in its rest-frame 0.24–11.8 keV energy band (or the observer-frame 0.2–10 keV energy band). The luminosities were obtained based on the fit to X1 with a multicolor disk (MCD) subject to a fast-moving warm absorber (Section 3.3) and adopting a distance of $D_L = 866$ Mpc (Section 3.1). The source was not detected in observation C1 in 2000 April, with $L_X < 4.1 \times 10^{41}$ (the 90% confidence upper bound; the same below; Table 1). The source was detected in X1 4.7 months later, with $L_X \sim 5.3 \times 10^{43}$ erg s⁻¹. In S1 in 2005 September, the source was not detected, with $L_X < 4.2 \times 10^{42}$ erg s⁻¹. It was not detected either in X2 in 2014 January, with $L_X < 2.1 \times 10^{41}$ erg s⁻¹. There-

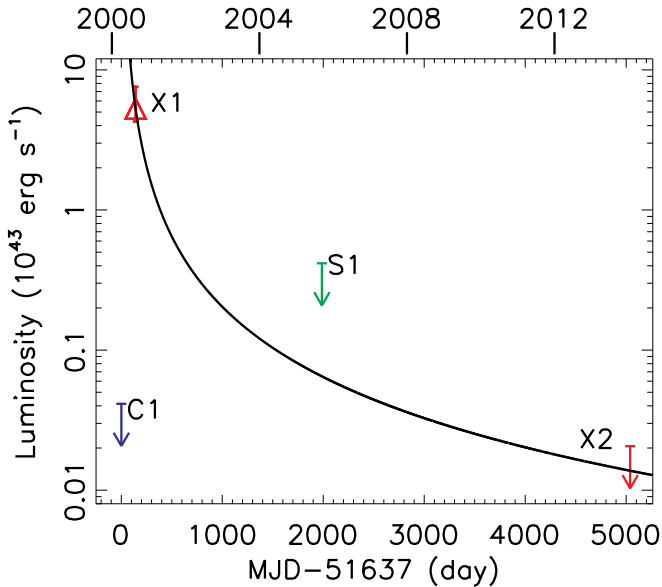


FIG. 3.— The long-term unabsorbed luminosity curve in the rest-frame 0.24–11.8 energy band. The uncertainties and upper bounds are at the 90% confidence level (see Table 1). The observations are noted in the plot. The solid line represents a $(t - t_D)^{-5/3}$ decline, assuming that X1 is on it and that the disruption time t_D is at the time of C1 (i.e., 4.7 months before X1).

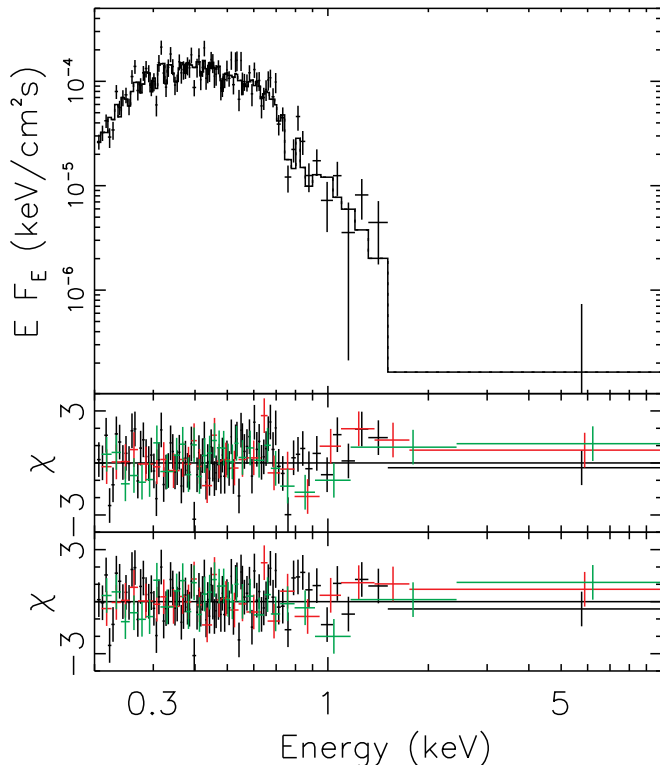


FIG. 4.— (top panel) The unfolded spectrum of X1 (for clarity, only the pn spectrum is shown). The spectrum was fitted with the MCD model subject to a fast-moving warm absorber (solid line). (middle panel and bottom panel) The fit residuals with the MCD model without and with the warm absorber, respectively (pn in black, MOS1 in red, and MOS2 in green). For clarity, the spectrum was rebinned to be above 1σ per bin in the plot.

fore the source has a long-term variability factor of $\gtrsim 260$. Figure 3 does not include the *ROSAT* observations. We

estimated L_X in R1 and R2 to be $< 1.9 \times 10^{42}$ erg s $^{-1}$ and $< 3.3 \times 10^{42}$ erg s $^{-1}$, thus a factor of > 28 and > 16 lower than that in X1, respectively.

In the UV and optical, the source was detected in the B and V filters, but not in other filters, in X1 and X2 (Table 2). The optical fluxes in these two *XMM-Newton* observations are consistent with each other and the SDSS measurements ($u' = 22.4 \pm 0.4$ mag, $g' = 21.09 \pm 0.05$ mag, $r' = 19.96 \pm 0.02$ mag, $i' = 19.51 \pm 0.02$ mag, and $z' = 19.17 \pm 0.06$ mag). In the *UVW1* filter in S1, there is no clear UV emission from J1521+0749 either, except some contamination from the read-out streak of a bright source. Although we obtained the *UVW1* AB magnitude of 23.3 ± 0.3 mag for J1521+0749 using *wotsource*, this value should be viewed as an upper limit. Therefore we observed no clear UV/optical variability accompanying the X-ray flare detected in X1.

3.3. Modeling of the X-ray Spectrum in X1

We fitted the X1 spectrum with several common simple models. To check the quality of the fits, we rebinned the spectrum to have a minimum of 20 count per bin and adopted the χ^2 statistic in the fits. However, all the best-fitting parameters that we will present were obtained from the final fits to the spectrum that were rebinned to have a minimum of one count per bin and adopted the C statistic, considering that the spectrum most likely include narrow absorption lines. The fits using the C statistic gave smaller uncertainties of the parameters than those using the χ^2 statistic, but they are consistent with each other within the uncertainties. Because our source is most likely associated with SDSS J152130.72+074916.5 at $z = 0.17901$ (Section 3.1), we applied this redshift to the spectral models with the convolution model *zshift* in XSPEC. All models included the Galactic absorption which we fixed at $N_H = 2.61 \times 10^{20}$ cm $^{-2}$ (Kalberla et al. 2005) using the *tbabs* model. We also included possible absorption intrinsic to the source using the *ztbabs* model. The abundance tables of Wilms et al. (2000) were used.

We first fitted the spectrum with a power law (PL) and obtained an unphysically high photon index of $\Gamma_{PL} = 5.9 \pm 0.2$ (the uncertainties from the spectral fits throughout the paper are all at the 90% confidence level), indicating an ultrasoft source. However, the fit is not acceptable, with the reduced χ^2 value of $\chi^2_\nu = 1.63$ for degrees of freedom $\nu = 147$. The fits with a MCD model (*diskbb* in XSPEC) is much better, with $\chi^2_\nu = 1.18$. However, clear residuals are seen between 0.5–1 keV (middle panel in Figure 4). We investigated several scenarios to explain the residuals. We first tried to add a PL. The fit was only marginally improved (at the 90% significance level), if we fixed Γ_{PL} at 2.0 and 3.0, with the PL contributing $< 2\%$ and $< 4\%$ (2σ upper limit) of the rest-frame 0.24–11.8 keV unabsorbed luminosity, respectively. We next tried the emission line explanation for the residuals by adding a Gaussian line (*gaussian* in XSPEC) to the MCD model. We obtained a significantly improved fit with $\chi^2_\nu = 1.09$ for $\nu = 144$ (i.e., a total decrease of χ^2 of 17.8 for three more degrees of freedom compared with the MCD fit). The final fit using the C statistic is given in Table 3. The line has a centroid rest-frame energy $E_{ga} = 0.75^{+0.02}_{-0.07}$ keV and a width $\sigma_{ga} = 0.02^{+0.06}$ keV, and the apparent in-

ner disk temperature is $kT_{\text{MCD}} = 0.125 \pm 0.006$ keV. The neutral absorption is negligible, which is also the case for all models tested below.

We then checked whether the residuals could be due to ionized absorption by applying the *edge* model on the MCD model and obtained a good fit with $\chi^2_\nu = 1.05$ ($\nu = 145$), i.e. χ^2 reduced by 22.5 (or the C statistic reduced by 27.2) for two more degrees of freedom. The final fit using the C statistic is given in Table 3. The edge energy is $E_{\text{edge}} = 0.85 \pm 0.02$ keV (rest-frame), and optical depth is $\tau_{\text{edge}} = 1.0 \pm 0.3$. The apparent inner disk temperature is now $kT_{\text{MCD}} = 0.144 \pm 0.007$ keV. To obtain the confidence level of the improvement of the fit from adding the *edge* model, we applied the posterior predictive *p*-value method (Hurkett et al. 2008; Protassov et al. 2002). With 10,000 spectra simulated, we found none having the reduction of the C statistic from the introduction of the *edge* model to be as large as obtained for the X1 spectrum (i.e., 27.2). Therefore the chance probability of improving the fit by adding the *edge* model is $< 10^{-4}$.

We tried to replace the *edge* model with the more physical warm absorber model *zxcipcf* (Reeves et al. 2008). We obtained a good fit with $\chi^2_\nu = 1.04$ ($\nu = 144$). The final fit using the C statistic is given in Table 3. The warm absorber has $N_{\text{H}} = (5^{+3}_{-1}) \times 10^{22}$ cm $^{-2}$, the ionization parameter $\log \xi = 2.0 \pm 0.1$, and an outflow line-of-sight velocity of $(0.12 \pm 0.02)c$, where c is the speed of light. The apparent inner disk temperature is slightly higher than inferred from the models investigated above ($kT_{\text{MCD}} = 0.17 \pm 0.02$ keV). The fit and the corresponding residuals, using the χ^2 statistic, are shown in the top and bottom panels in Figure 4, respectively. For this model, we checked the possible presence of a PL component and found it to improve the fit only at the 90% confidence level and contribute $< 4\%$ and $< 12\%$ (2σ upper limit) of the rest-frame 0.24–11.8 keV unabsorbed luminosity, if we fixed Γ_{PL} at 2.0 and 3.0, respectively.

Ultrasoft X-ray spectra are also often fitted with a single-temperature blackbody (BB, *bbodyrad* in XSPEC), and our fits with this model are given in Table 3. Because the residuals in 0.5–1 keV seen in the MCD fit are also present in the BB fit, we also tried a Gaussian line, an edge and a warm absorber to account for them. Generally, the fits using a BB have a χ^2 value higher by 4–8 than those using a MCD. The BB temperatures inferred are in the range between 0.10–0.13 keV.

Finally, we roughly estimated the BH mass with the AGN spectral model *optxagnf* (in XSPEC) by Done et al. (2012), assuming that the X1 spectrum is due to pure thermal disk emission (subject to a warm absorber). We note that *optxagnf* was created assuming a disk inclination of 60° . Table 3 gives the results of two fits, one for a non-rotating Schwarzschild BH and the other for a maximally rotating Kerr BH. The former inferred the BH mass of $(1.9 \pm 0.4) \times 10^5 M_\odot$ and the Eddington ratio of $4.2^{+1.9}_{-1.0}$, while the latter inferred the mass of $(1.4 \pm 0.3) \times 10^6 M_\odot$ and the Eddington ratio of $0.51^{+0.28}_{-0.12}$. The quality of both fits is as good as that we obtained with the MCD model, as indicated by the χ^2 value.

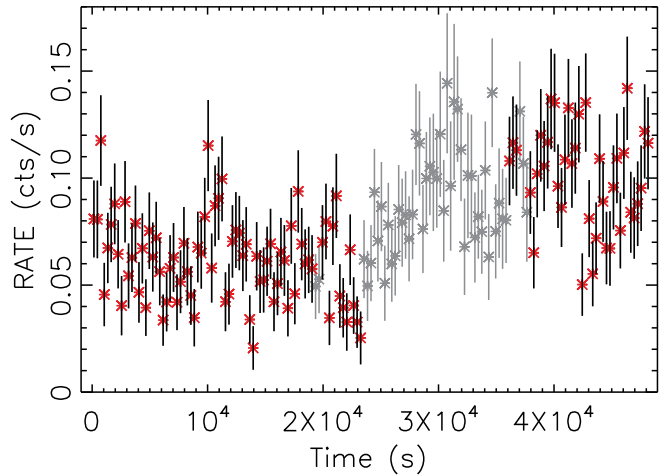


FIG. 5.— The observer-frame 0.2–2 keV pn background subtracted light curve from X1 created with the SAS tool *epiclccorr*. The bin size is 300 s. Data in the strong flare background intervals in the middle of the observation are shown in gray and seem to smoothly connect the data before and after the background flare.

3.4. The Short-term Variability in X1

Figure 5 shows the observer-frame 0.2–2 keV pn light curves binned at 300 s from X1. The source is clearly brighter at the end of the observation than at the beginning. The probability that the count rate is constant (excluding the high background flaring period) is 10^{-14} , from the χ^2 test. There may be fast variations by a factor of ~ 2 on timescales of thousands of seconds, such as those at 2.2×10^4 s and 4.3×10^4 s into the observation. We extracted a low-state spectrum from the first 28 ks of the observation and a high-state spectrum from the last 14 ks of the observation, excluding data in the high background intervals, and obtained the 0.6–1.2 keV to 0.2–0.6 keV pn count rate ratio to be 0.157 ± 0.015 and 0.262 ± 0.021 , respectively. Therefore the spectrum is softer at lower flux, at the 4.1σ significance level.

We fitted these low-state and high-state spectra with the MCD model subject to a fast-moving warm absorber (Section 3.3). The chance probability of improving the fit by adding the warm absorber is still low, 0.0003 and 0.001 for the low-state and high-state spectra, respectively, based on the posterior predictive *p*-value method using 10,000 simulations for each spectrum. The parameters of the neutral and ionized absorption were consistent with and thus fixed at values inferred from the fit to the average spectrum of the whole observation. We obtained the disk parameters $kT_{\text{MCD}} = 0.156 \pm 0.008$ keV and $N_{\text{MCD}} = 93^{+23}_{-19}$ for the low-state spectrum and $kT_{\text{MCD}} = 0.189 \pm 0.010$ keV and $N_{\text{MCD}} = 60^{+16}_{-12}$ for the high-state spectrum. The disk temperatures differ by 33 eV at the 4.3σ confidence level, while the inner disk radii differ by 24% at the 2.2σ confidence level. The mass accretion rates, $\dot{M} \propto T_{\text{MCD}}^4 N_{\text{MCD}}^{3/2}$ for the MCD model, differ by 11%, less than 1σ uncertainty (we used the XSPEC command *steppar* on T_{MCD} and N_{MCD} to calculate the uncertainty of \dot{M}). Therefore one explanation for the short-term variability in X1 is fast change of the inner disk radius at an approximately constant mass accretion rate into the disk. Figure 5 shows that the change occurred within ~ 10 ks.

4. DISCUSSION AND CONCLUSIONS

J1521+0749 is an ultrasoft X-ray transient consistent with the center of a galaxy at $z = 0.17901$. This galaxy is consistent with an old ($\gtrsim 10$ Gyr), passive stellar population, based on our modeling of its SDSS spectrum, which shows no clear emission lines. The 3σ upper limit of the bolometric luminosity of the persistent nuclear activity estimated from the [O III] upper limit is nearly three orders of magnitude lower than the peak X-ray luminosity in X1. Therefore we disfavor AGN activity as the explanation for the X-ray flare. Instead, it is a good soft TDE candidate. We only have one X-ray detection (X1), which does not allow us to formally test whether the event follows a $t^{-5/3}$ decline. However, we have a deep observation C1 relatively close to X1 (i.e., 4.7 months before X1), and the non-detection of the source in that observation allows us to constrain the disruption time t_D to be close to or after C1. In Figure 3, we plot a possible $(t - t_D)^{-5/3}$ decay curve, with t_D assumed to be at the time of C1. The non-detection limits of our source in S1 and X2, the latter of which is relatively deep, are consistent with this curve.

We fortunately caught the X-ray flare in a deep observation (X1). We detected short-term flux and spectral variability in X1, with the X-ray spectrum being softer at lower flux. Based on our spectral modeling, the variability could be due to change in the inner disk truncation radius, by 24% within ~ 10 ks, at a constant mass accretion rate. The variation timescale is thus 40 ks, close to the viscosity timescale at the innermost stable circular orbit, which is ~ 70 ks, assuming a viscosity parameter of 0.1, a ratio of the disk thickness to the inner disk radius of 0.1, and a BH mass of $10^6 M_\odot$ (see Equation 5.69 in Frank et al. 2002). Therefore the short-term variability in X1 could be due to viscosity instability of the disk. Another soft TDE candidate 2XMMi J184725.1-631724 that we discovered in Lin et al. (2011) also showed strong short-term variability in two deep *XMM-Newton* observations in the flare peak. We suggested the cause of its short-term variability to be the fast change in the mass accretion rate, considering the increase of the inner disk temperature with the flux as inferred from the fits to a low-state spectrum and a high-state spectrum in the second (brighter) *XMM-Newton* observation. We revisit this problem using the procedure as we adopted for J1521+0749, by calculating the mass accretion rate directly through $\dot{M} \propto T_{\text{MCD}}^4 N_{\text{MCD}}^{3/2}$ for the MCD when fitting the low-state and high-state spectra of the second *XMM-Newton* observation and fixing the absorption column density at the value inferred from the fit to the average spectrum from the whole observation (In Lin et al. (2011), we allowed the column density to be free but tied between the two spectra in fits; fixing the column density instead allows to obtain better constraints on the MCD parameters and thus more accurate comparison between the two spectra). In this way the disk temperatures of the low-state and high-state spectra were found to differ by 10 eV at the 7.9σ confidence level, the inner disk radii by 17% at the 3.3σ confidence level, and the mass accretion rates by 1%, less than 1σ uncertainty. Therefore the short-term variability in 2XMMi J184725.1-631724 could also be due to change in the inner disk truncation radius at a constant mass accretion rate caused by disk insta-

bility, as we suggest for J1521+0749. The TDE candidate SDSS J120136.02+300305.5 also showed short-term variability, but its cause is not clear (Saxton et al. 2012). Galactic stellar-mass BH X-ray binaries in the thermal disk dominated state tend to show very weak short-term variability (Remillard & McClintock 2006). The short-term variability could be a unique phenomenon for soft TDEs.

We also detected some edge residuals in 0.5–1 keV when fitting the X1 spectrum with a MCD. One explanation for them is the presence of a fast-moving warm absorber. This absorber could be the radiation-driven outflow expected when the stellar debris fallbacks and accretes onto the BH at a super-Eddington rate (Rees 1988; Strubbe & Quataert 2009, 2011; Lodato & Rossi 2011). In SDSS J120136.02+300305.5, Saxton et al. (2012) also detected an edge, at ~ 0.66 keV, whose cause is not clear.

We did not detect UV or optical variability between X1 and X2. Although we expect strong UV/optical emission from the disk and the outflow in the flare peak, such emission could be still too faint to be detected, maybe because our OM observations are not very deep and/or the galactic stellar emission is too strong. Based on Lodato & Rossi (2011), the peak g -band (close to the OM B filter) emission has the AB magnitude about 22.3 mag for a TDE of M_{BH} within 10^5 – $10^6 M_\odot$ at the distance of J1521+0749 (i.e., $D_L = 866$ Mpc), while the galaxy has a B -band magnitude of 21.2 ± 0.4 based on the X2 observation (Table 2). The disk UV/optical emission can also be estimated from modeling the X-ray spectrum of X1. For this, it is very important to take into account the irradiation of the outer disk by the inner disk emission. Therefore we adopted the irradiated disk model *diskir* in XSPEC (Gierliński et al. 2009). We assumed pure thermal disk emission, as the Compton tail was found to be very weak. The reddening relation $E(B - V) = 1.7 \times 10^{-22} N_{\text{H}}$ was adopted. The warm absorber was also required in the fit, but it was assumed to be dust-free. The outer disk radius was set to be 1000 times of the inner disk radius, which corresponds to ~ 100 times of the tidal disruption radius for a BH of $10^6 M_\odot$ (Guillochon et al. 2014). The fraction of bolometric flux thermalized in the outer disk f_{out} is assumed to be 0.1, which is unfeasibly large (f_{out} is typically $\sim 10^{-3}$ in stellar-mass BH X-ray binaries, Gierliński et al. 2009). Even adopting the above assumptions that favor the UV/optical emission, we still found that such emission is about one order of magnitude fainter than the galaxy emission (or the detection limit) in the OM filters used in X1 (Table 2).

Because of the super-Eddington accretion in TDEs, relativistic outflows could be launched and interact with interstellar medium, resulting in transient radio synchrotron emission that peaks at ~ 0.1 – 1 mJy (if the source is within Gpc distances) in ~ 1 yr after the disruption (Giannios & Metzger 2011; Bower 2011). However, despite discovery of two jetted hard TDE candidates, there is no clear evidence that soft TDEs also launch relativistic jets, because, thus far, there is no radio detection that can be unambiguously ascribed to a relativistic jet in soft TDEs (see Komossa 2015, for a review). We searched the Very Large Array (VLA) archival images and found only one after 2000 April when our event oc-

curred. It was taken on 2000 August 8 (close to X1 in time) in the L band (1.4 GHz). Our source was not detected, with 3σ upper limit about 0.8 mJy (three times the rms value at the location of our source). The non-detection is not constraining because the radio emission from the jet, even if it was launched, should be still weak at the beginning of the flare (Giannios & Metzger 2011).

The relatively large positional uncertainty of J1521+0749 does not rule out that it resulted from disruption of a main-sequence star by a massive BH residing in an off-nuclear (projected offset <2 kpc) globular cluster in SDSS J152130.72+074916.5. However, this explanation should not be very promising because if the BH mass is $\sim 10^5$ – $10^6 M_\odot$ as inferred from the X-ray spectral fit (Section 3.3) the cluster might have a much higher mass (e.g., Portegies Zwart et al. 2004) and thus would be very rare, especially for a host that is not very massive. The rate of disrupting a normal star by a massive BH in a globular cluster is also predicted to be extremely low ($\lesssim 10^{-7}$ yr $^{-1}$ per globular cluster), especially at late times (>2 Gyr, Baumgardt et al. 2004).

The BH inferred for our source is relatively small but might still be a little too large for the white dwarf (WD) tidal disruption, which requires the BH mass to be $\lesssim 2 \times 10^5 M_\odot$ if the disruption needs to be outside the event horizon or smaller if the disruption is desired to be outside the innermost stable circular orbit (e.g., Krolik & Piran 2011). The WD TDE is more prone to produce an energetic jet, thus hard X-ray emission, than the main-sequence star TDE, because the high density of WDs can support a strong magnetic field on the BH (Krolik & Piran 2011). Even in the case of a slow jet when the emission could be dominated by the jet photospheric thermal emission, the spectrum is unlikely to be as soft as in J1521+0749, due to Comptonization and broadening with pair production (Shcherbakov et al. 2013). Based on the above considerations, we disfavor the WD TDE explanation for J1521+0749.

The supersoft X1 spectrum of J1521+0749 is hardly seen in GRBs, even for the small ultralong class. Only the ultralong GRB 060218 showed a similarly soft spectrum (photon index ~ 5.5 , Margutti et al. 2015). The main problem of associating J1521+0749 with an ultralong GRB is that its host is consistent with an early-type galaxy, while most ultralong GRBs have hosts showing intensive star forming activity (e.g., Levan et al. 2014). Our source is unlikely to be a SN, because SNe hardly have $L_X > 10^{42}$ erg s $^{-1}$ and supersoft X-ray spectra. While the shock breakout in SN 2008D had peak L_X similar to J1521+0749 and showed relatively soft spectra (maximum photon index ~ 3.2 , Soderberg et al. 2008), the event was short ($\lesssim 600$ s) and had a fast rise, exponential decay profile. In contrast, the X1 observation of J1521+0749 was long (~ 13 hrs) and had much more steady count rates (the second half of the observation had 0.2–2 keV pn count rates higher by 60% than those in the first half only). Although the shock breakout in a massive star explosion might last for hours (Nakar & Sari 2012), the X1 observation of J1521+0749 was still too long and had too steady count rates to be part of such an event; the old stellar environment of J1521+0749 also argues against the explanation of a massive star explosion.

J1521+0749 appears in the direction of the cluster of galaxies MKW 3s ($z = 0.045$). Its candidate host galaxy SDSS J152130.72+074916.5 is not a member of this cluster. J1521+0749 is relatively close to, but still too far away to be in, two galaxies in the cluster, SDSS J152131.80+074851.9 ($z = 0.04533$ or $d_L = 201$ Mpc) and SDSS J152134.15+074815.3 ($z = 0.04225$ or $d_L = 187$ Mpc, see Figure 1). We can rule out J1521+0749 as a coronally active star based on the ratio of the 0.2–12 keV maximum flux to the K -band flux, which is $\log(F_X/F_{\text{IR}}) = 1.05$ for J1521+0749, much higher than seen in coronally active stars ($\log(F_X/F_{\text{IR}}) \lesssim -0.9$, Lin et al. 2012). The ultrasoft spectrum makes J1521+0749 similar to supersoft X-ray sources (SSS; Kahabka & van den Heuvel 2006; Greiner 2000). They are mostly cooling white dwarfs (WDs; Kahabka & van den Heuvel 2006) or nuclear burning of the hydrogen-rich matter on the surface of a WD in the so-called close binary supersoft sources or supersoft novae (Kahabka & van den Heuvel 2006; Greiner 2000). J1521+0749 is unlikely to be a cooling WD due to its large variability (Yungelson et al. 1996). It is unlikely to be a close binary supersoft source or a supersoft novae either, because such objects are uncommon (only a few tens found in our Galaxy, Kahabka & van den Heuvel 2006; Greiner 2000) and the chance to find one consistent with the center of a bright galaxy is essentially zero.

Therefore J1521+0749 is best explained as a soft TDE. Its high-quality X-ray data in X1 have allowed us to search for short-term variability and carry out detailed spectral modeling, which revealed rich information of the accretion process in the event. Few TDE candidates have such high-quality X-ray data. More soft TDEs of similar quality are needed to check whether the short-term variability and the edge that we detected in J1521+0749 are common in such events and to understand their origins.

We thank the anonymous referee for the helpful comments. We thank Andrej Lobanov for a critical reading of the manuscript. This work is partially supported by NASA ADAP Grant NNX10AE15G.

Funding for SDSS-III has been provided by the Alfred P. Sloan Foundation, the Participating Institutions, the National Science Foundation, and the U.S. Department of Energy Office of Science. The SDSS-III web site is <http://www.sdss3.org/>. SDSS-III is managed by the Astrophysical Research Consortium for the Participating Institutions of the SDSS-III Collaboration including the University of Arizona, the Brazilian Participation Group, Brookhaven National Laboratory, Carnegie Mellon University, University of Florida, the French Participation Group, the German Participation Group, Harvard University, the Instituto de Astrofísica de Canarias, the Michigan State/Notre Dame/JINA Participation Group, Johns Hopkins University, Lawrence Berkeley National Laboratory, Max Planck Institute for Astrophysics, Max Planck Institute for Extraterrestrial Physics, New Mexico State University, New York University, Ohio State University, Pennsylvania State University, University of Portsmouth, Princeton University, the Spanish Participation Group, University of Tokyo, University of Utah, Vanderbilt University, University of Virginia, University

of Washington, and Yale University.

REFERENCES

- Abazajian, K. N., Adelman-McCarthy, J. K., Agüeros, M. A., et al. 2009, *ApJS*, 182, 543
- Baumgardt, H., Makino, J., & Ebisuzaki, T. 2004, *ApJ*, 613, 1143
- Bautz, M. W., Pivovarov, M., Baganoff, F., et al. 1998, in *Society of Photo-Optical Instrumentation Engineers (SPIE) Conference Series*, Vol. 3444, *Society of Photo-Optical Instrumentation Engineers (SPIE) Conference Series*, ed. R. B. Hoover & A. B. Walker, 210–224
- Bloom, J. S., Giannios, D., Metzger, B. D., et al. 2011, *Science*, 333, 203
- Boulade, O., Charlot, X., Abbon, P., et al. 2003, in *Society of Photo-Optical Instrumentation Engineers (SPIE) Conference Series*, Vol. 4841, *Instrument Design and Performance for Optical/Infrared Ground-based Telescopes*, ed. M. Iye & A. F. M. Moorwood, 72–81
- Bower, G. C. 2011, *ApJ*, 732, L12
- Bruzual, G. & Charlot, S. 2003, *MNRAS*, 344, 1000
- Burrows, D. N., Hill, J. E., Nousek, J. A., et al. 2005, *Space Sci. Rev.*, 120, 165
- Burrows, D. N., Kennea, J. A., Ghisellini, G., et al. 2011, *Nature*, 476, 421
- Cappellari, M. & Emsellem, E. 2004, *PASP*, 116, 138
- Cenko, S. B., Krimm, H. A., Horesh, A., et al. 2012, *ApJ*, 753, 77
- Donato, D., Cenko, S. B., Covino, S., et al. 2014, *ApJ*, 781, 59
- Done, C., Davis, S. W., Jin, C., Blaes, O., & Ward, M. 2012, *MNRAS*, 420, 1848
- Esquej, P., Saxton, R. D., Komossa, S., et al. 2008, *A&A*, 489, 543
- Frank, J., King, A., & Raine, D. J. 2002, *Accretion Power in Astrophysics: Third Edition*, ed. J. Frank, A. King, & D. J. Raine
- Giannios, D. & Metzger, B. D. 2011, *MNRAS*, 416, 2102
- Gierliński, M., Done, C., & Page, K. 2009, *MNRAS*, 392, 1106
- Graham, A. W. 2007, *MNRAS*, 379, 711
- Graham, A. W. & Scott, N. 2015, *ApJ*, 798, 54
- Greiner, J. 2000, *New Astronomy*, 5, 137
- Grupe, D., Burrows, D. N., Wu, X.-F., et al. 2010, *ApJ*, 711, 1008
- Grupe, D., Nousek, J. A., Veres, P., Zhang, B.-B., & Gehrels, N. 2013, *ApJS*, 209, 20
- Grupe, D., Thomas, H., & Leighly, K. M. 1999, *A&A*, 350, L31
- Guillochon, J., Manukian, H., & Ramirez-Ruiz, E. 2014, *ApJ*, 783, 23
- Gwyn, S. D. J. 2008, *PASP*, 120, 212
- Hurkett, C. P., Vaughan, S., Osborne, J. P., et al. 2008, *ApJ*, 679, 587
- Immler, S. 2007, in *American Institute of Physics Conference Series*, Vol. 937, *Supernova 1987A: 20 Years After: Supernovae and Gamma-Ray Bursters*, ed. S. Immler, K. Weiler, & R. McCray, 246–255
- Jansen, F., Lumb, D., Altieri, B., et al. 2001, *A&A*, 365, L1
- Kahabka, P. & van den Heuvel, E. P. J. 2006, *Super-soft sources*, ed. Lewin, W. H. G. & van der Klis, M., 461–474
- Kalberla, P. M. W., Burton, W. B., Hartmann, D., et al. 2005, *A&A*, 440, 775
- Komossa, S. 2012, in *European Physical Journal Web of Conferences*, Vol. 39, *European Physical Journal Web of Conferences*, 2001
- Komossa, S. 2015, arXiv:1505.01093, *Journal of High Energy Astrophysics*, in press
- Komossa, S. & Bade, N. 1999, *A&A*, 343, 775
- Komossa, S. & Greiner, J. 1999, *A&A*, 349, L45
- Krolik, J. H. & Piran, T. 2011, *ApJ*, 743, 134
- Lamastra, A., Bianchi, S., Matt, G., et al. 2009, *A&A*, 504, 73
- Lawrence, A., Warren, S. J., Almaini, O., et al. 2007, *MNRAS*, 379, 1599
- Levan, A. J., Read, A. M., Metzger, B. D., Wheatley, P. J., & Tanvir, N. R. 2013, *ApJ*, 771, 136
- Levan, A. J., Tanvir, N. R., Starling, R. L. C., et al. 2014, *ApJ*, 781, 13
- Lidskii, V. V. & Ozernoi, L. M. 1979, *Soviet Astronomy Letters*, 5, 16
- Lin, D., Carrasco, E. R., Grupe, D., et al. 2011, *ApJ*, 738, 52
- Lin, D., Webb, N. A., & Barret, D. 2012, *ApJ*, 756, 27
- . 2014, *ApJ*, 780, 39
- Lodato, G. & Rossi, E. M. 2011, *MNRAS*, 410, 359
- Maksym, W. P., Lin, D., & Irwin, J. A. 2014a, *ApJ*, 792, L29
- Maksym, W. P., Ulmer, M. P., & Eracleous, M. 2010, *ApJ*, 722, 1035
- Maksym, W. P., Ulmer, M. P., Eracleous, M. C., Guennou, L., & Ho, L. C. 2013, *MNRAS*, 435, 1904
- Maksym, W. P., Ulmer, M. P., Roth, K. C., et al. 2014b, *MNRAS*, 444, 866
- Marconi, A. & Hunt, L. K. 2003, *ApJ*, 589, L21
- Margutti, R., Guidorzi, C., Lazzati, D., et al. 2015, *ApJ*, 805, 159
- Mason, K. O., Breeveld, A., Much, R., et al. 2001, *A&A*, 365, L36
- Nakar, E. & Sari, R. 2012, *ApJ*, 747, 88
- Piro, L., Troja, E., Gendre, B., et al. 2014, *ApJ*, 790, L15
- Portegies Zwart, S. F., Baumgardt, H., Hut, P., Makino, J., & McMillan, S. L. W. 2004, *Nature*, 428, 724
- Protassov, R., van Dyk, D. A., Connors, A., Kashyap, V. L., & Siemiginowska, A. 2002, *ApJ*, 571, 545
- Rees, M. J. 1988, *Nature*, 333, 523
- . 1990, *Science*, 247, 817
- Reeves, J., Done, C., Pounds, K., et al. 2008, *MNRAS*, 385, L108
- Remillard, R. A. & McClintock, J. E. 2006, *ARA&A*, 44, 49
- Roming, P. W. A., Kennedy, T. E., Mason, K. O., et al. 2005, *Space Sci. Rev.*, 120, 95
- Rosen, S. R., Webb, N. A., Watson, M. G., et al. 2015, arXiv:1504.07051
- Rots, A. H. & Budavári, T. 2011, *ApJS*, 192, 8
- Saxton, R. D., Read, A. M., Esquej, P., et al. 2012, *A&A*, 541, A106
- Shcherbakov, R. V., Pe'er, A., Reynolds, C. S., et al. 2013, *ApJ*, 769, 85
- Soderberg, A. M., Berger, E., Page, K. L., et al. 2008, *Nature*, 453, 469
- Strubbe, L. E. & Quataert, E. 2009, *MNRAS*, 400, 2070
- . 2011, *MNRAS*, 415, 168
- Strüder, L., Briel, U., Dennerl, K., et al. 2001, *A&A*, 365, L18
- Turner, M. J. L., Abbey, A., Arnaud, M., et al. 2001, *A&A*, 365, L27
- Vazdekis, A., Sánchez-Blázquez, P., Falcón-Barroso, J., et al. 2010, *MNRAS*, 404, 1639
- Watson, M. G., Schröder, A. C., Fyfe, D., et al. 2009, *A&A*, 493, 339
- Wilms, J., Allen, A., & McCray, R. 2000, *ApJ*, 542, 914
- Yungelson, L., Livio, M., Truran, J. W., Tutukov, A., & Fedorova, A. 1996, *ApJ*, 466, 890